Circular dielectric cavity and its deformations

R. Dubertrand,[1,*] E. Bogomolny,[1] N. Djellali,[2] M. Lebental,[1,2] and C. Schmit[1,†]
[1]*Université Paris Sud, CNRS UMR 8626, Laboratoire de Physique Théorique et Modèles Statistiques, 91405 Orsay, France*
[2]*Ecole Normale Supérieure de Cachan, CNRS UMR 8537, Laboratoire de Photonique Quantique et Moléculaire, 94235 Cachan, France*
(Received 30 August 2007; published 9 January 2008)

The construction of perturbation series for slightly deformed dielectric circular cavity is discussed in detail. The obtained formulas are checked on the example of cut disks. A good agreement is found with direct numerical simulations and far-field experiments.

DOI: 10.1103/PhysRevA.77.013804 PACS number(s): 42.55.Sa, 03.65.Sq

I. INTRODUCTION

Dielectric microcavities are now widely used as microresonators and microlasers in different physical, chemical, and biological applications (see, e.g., [1,2] and references therein). The principal object of these studies is the optical emission from thin dielectric microcavities of different shapes [3]. Schematically such cavity can be represented as a cylinder whose height is small in comparison with its transverse dimensions (see Fig. 1). If the refractive index of the cavity is n_1 and the cavity is surrounded by a material with the refractive index $n_2 < n_1$ (we assume that the permeabilities in both media are the same) the time-independent Maxwell's equations take the form (see, e.g., [4])

$$\vec{\nabla} \cdot \vec{B}_j = 0, \quad \vec{\nabla} \cdot n_j^2 \vec{E}_j = 0,$$

$$\vec{\nabla} \times \vec{B}_j = -i n_j^2 k \vec{E}_j, \quad \vec{\nabla} \times \vec{E}_j = ik\vec{B}_j, \tag{1}$$

where the subscript $j=1$ $(j=2)$ denotes points inside (outside) the cavity and k is the wave vector in the vacuum. These equations have to be completed by the boundary conditions which follow from the continuity of normal $\vec{B}_\nu$ and $n^2\vec{E}_\nu$ and tangential $\vec{E}_\tau$ and $\vec{B}_\tau$ components

$$n_1^2 \vec{E}_{1\nu} = n_2^2 \vec{E}_{2\nu}, \quad \vec{B}_{1\nu} = \vec{B}_{2\nu}, \quad \vec{E}_{1\tau} = \vec{E}_{2\tau}, \quad \vec{B}_{1\tau} = \vec{B}_{2\tau}.$$

In the true cylindrical geometry, the z dependence of electromagnetic fields is pure exponential: $\sim e^{iqz}$. Then the above Maxwell equations can be reduced to the two-dimensional Helmholtz equations for the electric field, E_{jz}, and the magnetic field B_{jz} along the axe of the cylinder

$$(\Delta + \tilde{n}_j^2 k^2) E_{jz}(x,y) = 0, \quad (\Delta + \tilde{n}_j^2 k^2) B_{jz}(x,y) = 0 \tag{2}$$

with the following boundary conditions

$$E_{1z} = E_{2z}, \quad B_{1z} = B_{2z}, \quad \frac{\partial E_{1z}}{\partial \tau} = \frac{\partial E_{2z}}{\partial \tau}, \quad \frac{\partial B_{1z}}{\partial \tau} = \frac{\partial B_{2z}}{\partial \tau},$$

and

$$\frac{1}{\tilde{n}_1^2}\frac{\partial B_{1z}}{\partial \nu} - \frac{1}{\tilde{n}_2^2}\frac{\partial B_{2z}}{\partial \nu} = \frac{q(n_2^2 - n_1^2)}{k\tilde{n}_1^2\tilde{n}_2^2}\frac{\partial E_z}{\partial \tau},$$

$$\frac{n_1^2}{\tilde{n}_1^2}\frac{\partial E_{1z}}{\partial \nu} - \frac{n_2^2}{\tilde{n}_2^2}\frac{\partial E_{2z}}{\partial \nu} = \frac{q(n_2^2 - n_1^2)}{k\tilde{n}_1^2\tilde{n}_2^2}\frac{\partial B_z}{\partial \tau}. \tag{3}$$

Here $\tilde{n}_j^2 = n_j^2 - q^2/k^2$ plays the role of the effective two-dimensional (in the x-y plane) refractive index.

When fields are independent on z (i.e., $q=0$) boundary conditions (3) do not mix B_z and E_z and the two polarizations are decoupled. They are called transverse electric (TE) field when $E_z=0$ and transverse magnetic (TM) field when $B_z=0$. Both cases are described by the scalar equations

$$(\Delta + \tilde{n}_j^2 k^2)\Psi_j(x,y) = 0, \tag{4}$$

where $\Psi(x,y)$ stands for electric (TM) or magnetic (TE) fields with the following conditions on the interface between both media: $\Psi_1 = \Psi_2$ and

$$\frac{\partial \Psi_1}{\partial \nu} = \frac{\partial \Psi_2}{\partial \nu} \quad \text{for TM polarization}, \tag{5}$$

$$\frac{1}{n_1^2}\frac{\partial \Psi_1}{\partial \nu} = \frac{1}{n_2^2}\frac{\partial \Psi_2}{\partial \nu} \quad \text{for TE polarization}. \tag{6}$$

These equations are, strictly speaking, valid only for an infinite cylinder but they are widely used for a thin dielectric cavities by introducing the effective refractive index corresponding to the propagation of confined modes in the bulk of the cavity (see, e.g., [5]). In practice, it reduces to small changes in the refractive indices (which nevertheless is of importance for careful comparison with experiment [6]). For simplicity, we will consider below two-dimensional equations (4) as the exact ones.

Only in very limited cases, these equations can be solved analytically. The most known case is the circular cavity (the

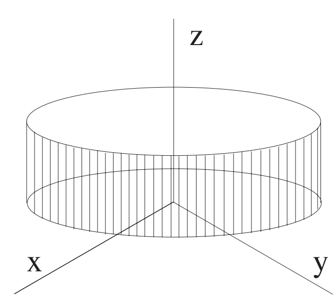

FIG. 1. Schematic representation of a dielectric cavity.

*remy.dubertrand@lptms.u-psud.fr
†Deceased.

disk) where variables are separated in polar coordinates. For other cavity shapes tedious numerical simulations are necessary.

The purpose of this paper is to develop perturbation series for quasistationary spectrum and corresponding wave functions for general cavities which are small deformations of the disk. The obtained formulas are valid when an expansion parameter is small enough. The simplicity, the generality, and the physical transparency of the results make such approach of importance for technological and experimental applications.

The plan of the paper is the following. In Sec. II the calculation of quasistationary states for a circular cavity is reviewed for completeness. Special attention is given to certain properties rarely mentioned in the literature. The construction of perturbation series for eigenvalues and eigenfunctions of small perturbations of circular cavity boundary is discussed in Sec. III. The conditions of applicability of perturbation expansions are discussed in Sec. IV. The obtained general formulas are then applied to the case of cut disks in Sec. V. Some technical details are collected in the Appendixes.

II. DIELECTRIC DISK

Let us consider a two-dimensional circular cavity of radius R made of a material with $n>1$ refractive index. The region outside the cavity is assumed to be the air with a refractive index of one. The two-dimensional equations (4) for this cavity are

$$(\Delta + n^2k^2)\Psi = 0 \quad \text{when } r \leqslant R,$$

$$(\Delta + k^2)\Psi = 0 \quad \text{when } r > R. \tag{7}$$

These equations describe the propagation of the electromagnetic field inside a dielectric cavity. They can also be considered as a quantum problem for a particle moving in the following "potential":

$$V(\vec{x}) = \begin{cases} -(n^2-1)k^2, & r \leqslant R \\ 0, & r > R, \end{cases}$$

and throughout this paper we will often refer to this analogy using vocabulary related to the quantum problem.

There is no true bound states for dielectric cavities. The physical origin of the existence of long lived quasibound states is the total internal reflection of rays with the incidence angle bigger than the critical angle

$$\theta_c = \arcsin\frac{1}{n}. \tag{8}$$

To investigate quasibound states one imposes outgoing boundary condition at infinity, namely, we require that far from the cavity there exist only outgoing waves

$$\Psi(\vec{x}) \propto e^{ik|\vec{x}|} \quad \text{when } |\vec{x}| \to \infty,$$

where $\vec{x}$ lies in the cavity plane.

In cylindrical coordinates (r,θ), the general form of the solutions is the following:

$$\Psi(r,\theta) = \begin{cases} a_m J_m(nkr)e^{im\theta}, & r \leqslant R \\ b_m H_m^{(1)}(kr)e^{im\theta}, & r > R, \end{cases} \tag{9}$$

where $m=0,1,\ldots$ is an integer (the azimuthal quantum number) related to the orbital momentum. $J_m(x)$ $[H_m^{(1)}(x)]$ stands for the Bessel function (the Hankel function of the first kind) of order m. Due to rotational symmetry, eigenvalues with $m \neq 0$ are doubly degenerated.

By imposing the boundary conditions (5) or (6) one gets the quantization condition

$$\frac{n}{\nu}\frac{J_m'}{J_m}(nkR) = \frac{H_m^{(1)\prime}}{H_m^{(1)}}(kR), \tag{10}$$

where

$$\nu = \begin{cases} 1 & \text{for TM polarization} \\ n^2 & \text{for TE polarization.} \end{cases} \tag{11}$$

The quasistationary eigenvalues of this problem depend on azimuthal quantum number m and on other quantum number p related with radial momentum: $k=k_{mp}$. They are complex numbers

$$k = k_r + ik_i, \tag{12}$$

where k_r determines the position of a resonance and $k_i<0$ is related with its lifetime.

In Fig. 2 we plot solutions of Eq. (10) obtained numerically for a circular cavity with refractive index $n=1.5$. Points are organized in families corresponding to different values of radial quantum number p. The dotted line in these figures indicates the classical lifetime of modes with fixed m and $k \to \infty$. Physically these modes correspond to waves propagating along the diameter whose lifetime is given by

$$\mathrm{Im}(kR) = \frac{1}{2n}\ln\left(\frac{n-1}{n+1}\right) \simeq -0.536\,48. \tag{13}$$

In the semiclassical limit and for $\mathrm{Im}(kR) \ll \mathrm{Re}(kR)$ simple approximate formulas can be obtained from the standard approximation of the Bessel and Hankel functions [7] when $m<z$,

$$J_m(z) = \sqrt{\frac{2}{\pi}}\frac{1}{(z^2-m^2)^{1/4}}\cos\left(\sqrt{z^2-m^2} - m\arccos\frac{m}{z} - \frac{\pi}{4}\right) \tag{14}$$

and when $m>z$,

$$H_m^{(1)}(z) = -i\sqrt{\frac{2}{\pi}}\frac{e^{-\sqrt{m^2-z^2}}}{(m^2-z^2)^{1/4}}\left[\frac{m}{z} + \sqrt{\left(\frac{m}{z}\right)^2 - 1}\right]^m. \tag{15}$$

Denoting $u=\mathrm{Re}(kR)$ and $v=\mathrm{Im}(kR)$ and assuming that $v \ll u$, $u \gg 1$, and $m/n<u<m$ one gets (see, e.g., [8]) that the

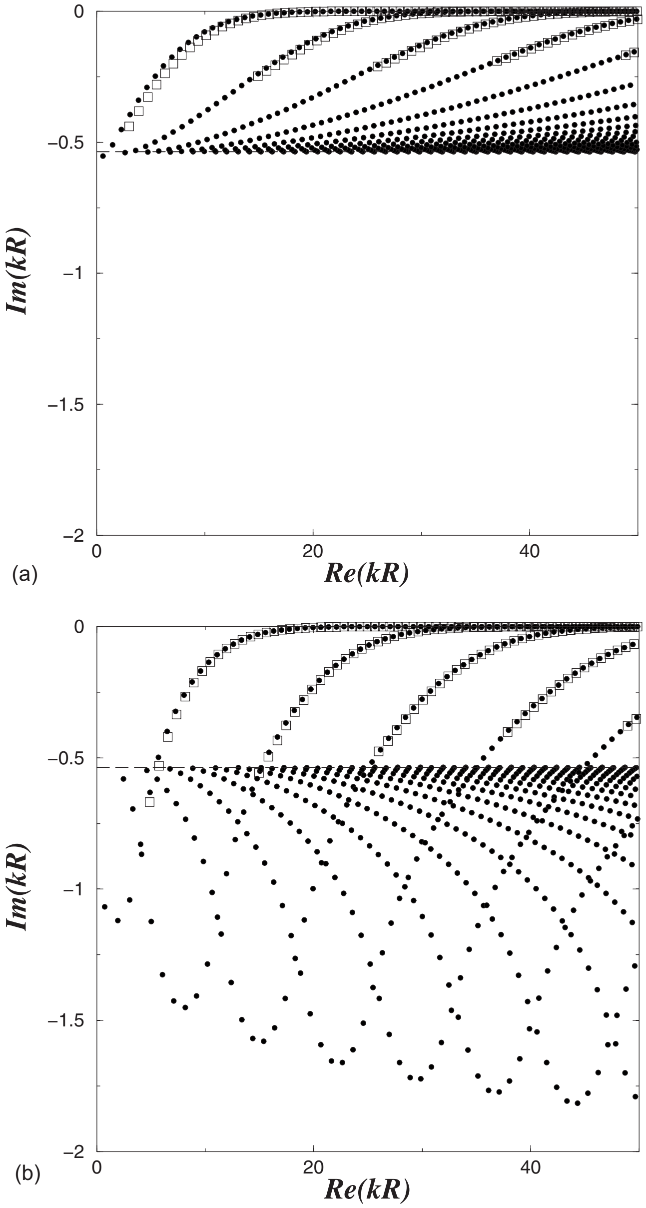

FIG. 2. Quasistationary eigenvalues for a circular cavity with $n=1.5$. (a) TM polarization; (b) TE polarization. Filled circles are deduced from direct numerical resolution of Eq. (10), while open squares indicate semiclassical approximation for these eigenvalues based on Eqs. (16) and (17) when $|kR|<m<n|kR|$.

real part of Eq. (10) can be transformed to the following form

$$\sqrt{n^2u^2-m^2} - m \arccos \frac{m}{nu} - \frac{\pi}{4} = \arctan \nu \sqrt{\frac{m^2-u^2}{n^2u^2-m^2}} + (p-1)\pi, \qquad (16)$$

where the integer $p=1,2,\ldots$ is the radial quantum number and ν is defined in Eq. (11). The imaginary part of Eq. (10) is then reduced to

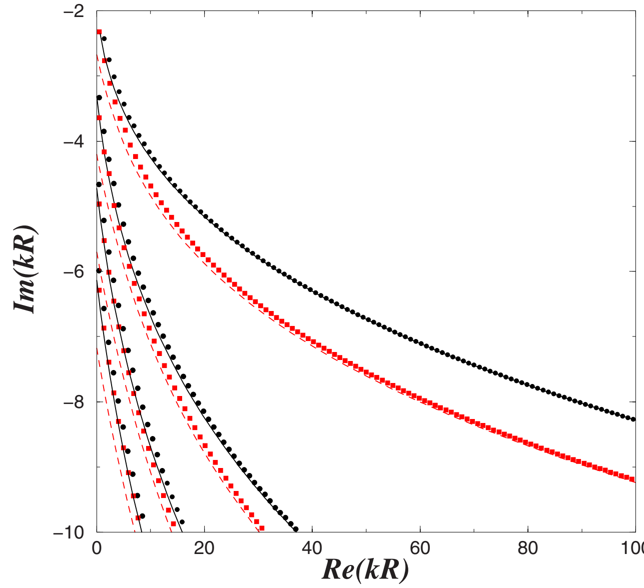

FIG. 3. (Color online) Additional branches of quasistationary eigenvalues for a circular cavity with $n=1.5$. Circles indicate the TM modes and squares show the position of the TE modes. Solid and dashed lines represent the asymptotic result (19) for respectively the TM and the TE modes.

$$v \approx -\frac{2}{\pi u(n^2-1)|H_m^{(1)}(u)|^2}\zeta, \qquad (17)$$

where $\zeta=1$ for TM waves and $\zeta=n^2u^2/[m^2(n^2+1)-n^2u^2]$ for TE waves. When u and m are large, v is exponentially small as it follows from Eq. (15).

The above equations cannot be applied for the most confined levels (similar to the "whispering gallery" modes in closed billiards) for which nu is close to m. In Appendix A it is shown that the real part of such quasi-stationary eigenvalues with $O(m^{-1})$ precision is given by the following expression

$$x_{m,p} = \frac{m}{n} + \frac{\eta_p}{n}\left(\frac{m}{2}\right)^{1/3} - \frac{1}{\nu\sqrt{n^2-1}} + \frac{3\eta_p^2}{20n}\left(\frac{2}{m}\right)^{1/3} + \frac{n^2\eta_p}{2\nu(n^2-1)^{3/2}}\left(\frac{2}{3\nu^2}-1\right)\left(\frac{2}{m}\right)^{2/3}, \qquad (18)$$

where η_p is the modulus of the pth zero of the Airy function (A2).

A more careful study of Eq. (10) reveals that there exist other branches of eigenvalues with large imaginary part not visible in Fig. 2. Some of them are indicated in Fig. 3. These states can be called external whispering gallery modes as their wave functions are practically zero inside the circle. So they are of minor importance for our purposes. They can also be identified with above-barrier resonances. In Appendix A it is shown that in the semiclassical limit these states are related with the complex zeros of the Hankel functions and they are well described asymptotically [with $O(m^{-1})$ error] as follows:

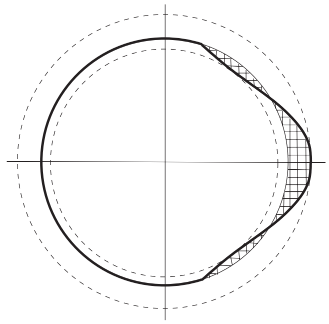

FIG. 4. Example of a deformed circular cavity. Shaded areas represent the regions where the refractive index differs from the one of the circular cavity.

$$x_{m,p} = m + \left(\frac{m}{2}\right)^{1/3} \eta_p e^{-2i\pi/3} - \frac{i\nu}{\sqrt{n^2-1}} + \frac{3e^{-4i\pi/3}\eta_p^2}{20}\left(\frac{2}{m}\right)^{1/3} + \frac{i\nu\eta_p e^{-2i\pi/3}}{2(n^2-1)^{3/2}}\left(1-\frac{2}{3}\nu^2\right)\left(\frac{2}{m}\right)^{2/3}, \qquad (19)$$

with the same η_p as in Eq. (18).

Similar equations have been obtained in [9].

III. PERTURBATION TREATMENT OF DEFORMED CIRCULAR CAVITIES

In the previous section we have considered the case of a dielectric circular cavity. It is one of the rare cases of integrable dielectric cavities in two dimensions. The purpose of this section is to develop a perturbation treatment for a general cavity shape which is a small deformation of the circle (see Fig. 4). We consider a cavity whose boundary is defined as

$$r = R + \lambda f(\theta) \qquad (20)$$

in the polar coordinates (r,θ). Here λ is a formal small parameter aiming at arranging perturbation series.

Our main assumption is that the deformation function $\lambda f(\theta)$ is small,

$$|\lambda f(\theta)| \ll R. \qquad (21)$$

Of course, for the quantum mechanical perturbation theory this condition is not enough. It is quite natural (and will be demonstrated below) that the criterion of applicability of the quantum perturbation theory is, roughly,

$$\delta a k^2 \ll 1, \qquad (22)$$

where δa is the area where perturbation "potential" δn^2 is nonzero (represented by dashed regions in Fig. 4).

To construct the perturbation series for the quasistationary states, we use two complementary methods. In Sec. III A we adapt the method proposed in [10,11] for diffraction problems. The main idea of this method is to impose the required boundary conditions (5) or (6) not along the true boundary of the cavity but on the circle $r=R$. Under the assumption (22) this task can be achieved by perturbation series in λ. In Sec. III B we use a more standard method based on the direct perturbation solution of the required equations using the Green function of the circular dielectric cavity. Both methods lead to the same series but they stress different points and may be useful in different situations.

For clarity we consider only the TM polarization where the field and its normal derivative are continuous on the dielectric interface. For the TE polarization the calculations are more tedious but follow the same steps. To simplify the discussion we assume that the deformation function $f(\theta)$ is symmetric: $f(-\theta)=f(\theta)$ (as in Fig. 4). In this case the quasistationary eigenfunctions are either symmetric or antisymmetric with respect to this inversion. Then in polar coordinates, they can be expanded either in $\cos(p\theta)$ or $\sin(p\theta)$ series. The general case of nonsymmetric cavities is analogous to the case of degenerate perturbation series and can be treated correspondingly.

A. Boundary shift

The condition of continuity of the wave function at the dielectric interface states

$$\Psi_1[R+\lambda f(\theta),\theta] = \Psi_2[R+\lambda f(\theta),\theta], \qquad (23)$$

where subscripts 1 and 2 refer respectively to wave function inside and outside the cavity. Expanding formally $\Psi_{1,2}$ into powers of λ one gets

$$[\Psi_1-\Psi_2](R,\theta) = -\lambda f(\theta)\left[\frac{\partial\Psi_1}{\partial r}-\frac{\partial\Psi_2}{\partial r}\right](R,\theta) - \frac{1}{2}\lambda^2 f^2(\theta) \times\left[\frac{\partial^2\Psi_1}{\partial r^2}-\frac{\partial^2\Psi_2}{\partial r^2}\right](R,\theta) + \cdots. \qquad (24)$$

For the TM polarization the conditions (5) imply that the derivatives of the wave functions inside and outside the cavity along any direction are the same. Choosing the radial direction, one gets the second boundary condition

$$\frac{\partial\Psi_1}{\partial r}[R+\lambda f(\theta),\theta] = \frac{\partial\Psi_2}{\partial r}[R+\lambda f(\theta),\theta], \qquad (25)$$

which can be expanded over λ as follows:

$$\left[\frac{\partial\Psi_1}{\partial r}-\frac{\partial\Psi_2}{\partial r}\right](R,\theta) = -\lambda f(\theta)\left[\frac{\partial^2\Psi_1}{\partial r^2}-\frac{\partial^2\Psi_2}{\partial r^2}\right](R,\theta) - \frac{1}{2}\lambda^2 f^2(\theta)\left[\frac{\partial^3\Psi_1}{\partial r^3}-\frac{\partial^3\Psi_2}{\partial r^3}\right](R,\theta) + \cdots. \qquad (26)$$

We find it convenient to look for the solutions of Eqs. (24) and (26) in the following form:

$$\Psi_1(r,\theta) = \frac{J_m(nkr)}{J_m(nx)}\cos(m\theta) + \sum_{p\neq m} a_p \frac{J_p(nkr)}{J_p(nx)}\cos(p\theta), \qquad (27)$$

$$\Psi_2(r,\theta) = (1+b_m)\frac{H_m^{(1)}(kr)}{H_m^{(1)}(x)}\cos(m\theta) + \sum_{p\neq m}(a_p+b_p)\frac{H_p^{(1)}(kr)}{H_p^{(1)}(x)}\cos(p\theta). \quad (28)$$

Here, and for all which follows, x stands for kR. These expressions correspond to symmetric eigenfunctions. For antisymmetric functions all $\cos(\cdots)$ have to be substituted by $\sin(\cdots)$.

From Eqs. (24) and (26) one concludes that the unknown coefficients a_p, and b_p have the following expansions:

$$a_p = \lambda\alpha_p + \lambda^2\beta_p + \cdots, \quad b_p = \lambda^2\gamma_p + \cdots. \quad (29)$$

Correspondingly, the quasistationary eigenvalue, $kR \equiv x$, can be represented as the following series

$$x = x_0 + \lambda x_1 + \lambda^2 x_2 + \cdots. \quad (30)$$

Here x_0 is the complex solution of Eq. (10) which we rewrite in the form

$$S_m(x_0) = 0 \quad (31)$$

introducing for a further use the notation for all m and x,

$$S_m(x) = n\frac{J_m'}{J_m}(nx) - \frac{H_m^{(1)\prime}}{H_m^{(1)}}(x). \quad (32)$$

The explicit construction of these perturbation series is presented in Appendix B. The results are the following. The perturbed eigenvalue (30) is

$$x = x_0\left[1 - \lambda A_{mm} + \lambda^2\left(\frac{1}{2}(3A_{mm}^2 - B_{mm}) + x_0(A_{mm}^2 - B_{mm}) \times\frac{H_m^{(1)\prime}}{H_m^{(1)}}(x_0) - (n^2-1)x_0\sum_{k\neq m}A_{mk}\frac{1}{S_k(x_0)}A_{km}\right)\right] + O(\lambda^3). \quad (33)$$

The coefficients of the quasistationary eigenfunction (27) and (28) are

$$a_p = \lambda x_0(n^2-1)\frac{1}{S_p(x_0)}\left(A_{pm} + \lambda\left\{A_{pm}A_{mm}\left(\frac{x_0}{S_p}\frac{\partial S_p}{\partial x} - 1\right) + \frac{1}{2}B_{pm}\left[1 + x_0\left(\frac{H_m^{(1)\prime}}{H_m^{(1)}} + \frac{H_p^{(1)\prime}}{H_p^{(1)}}\right)\right] + x_0(n^2-1) \times\sum_{k\neq m}A_{pk}\frac{1}{S_k(x_0)}A_{km}\right\}\right) + O(\lambda^3) \quad (34)$$

and

$$b_p = \lambda^2\frac{1}{2}x_0^2(n^2-1)B_{pm} + O(\lambda^3). \quad (35)$$

In these formulas A_{mn} and B_{mn} are the Fourier harmonics of the perturbation function $f(\theta)$ and its square, given by Eqs. (B5) and (B10), respectively. The above expressions are quite similar to usual perturbation series and $S_p(x_0)$ plays the role of the energy denominator. In Eq. (34) and in the following we may omit the argument of the function when it is equal to x_0.

It is instructive to calculate the imaginary part of the perturbed level from the knowledge of the first order terms only. Assuming that $\mathrm{Im}(x_0) \ll \mathrm{Re}(x_0)$ and using the Wronskian relation (see, e.g., [7], 7.11.34)

$$H_m^{(1)\prime}(x)H_m^{(2)}(x) - H_m^{(2)\prime}(x)H_m^{(1)}(x) = \frac{4i}{\pi x} \quad (36)$$

one gets from Eq. (33)

$$\mathrm{Im}(x) = \mathrm{Im}(x_0)(1+\rho) - \lambda^2\frac{2x_0(n^2-1)}{\pi}\sum_{p\neq m}\frac{A_{mp}^2}{|S_pH_p^{(1)}|^2}, \quad (37)$$

where [assuming that $m > x_0$ so $H_m^{(1)\prime}/H_m^{(1)}$ is real, cf. Eq. (15)]

$$\rho = -\lambda A_{mm} + \lambda^2\left[\frac{1}{2}(3A_{mm}^2 - B_{mm}) + x_0(A_{mm}^2 - B_{mm})\frac{H_m^{(1)\prime}}{H_m^{(1)}}(x_0)\right]. \quad (38)$$

Expression (37) without the ρ correction [which is multiplied by $\mathrm{Im}(x_0)$ and so negligible for well-confined levels] can be independently calculated from the following general considerations. From Eq. (7) it follows that inside the cavity

$$n^2(k^2 - k^{*2})\int_V|\Psi(\vec{x})|^2 d\vec{x} = J, \quad (39)$$

where

$$J = \int_B\left(\Psi^*\frac{\partial}{\partial\vec{\nu}}\Psi - \Psi\frac{\partial}{\partial\vec{\nu}}\Psi^*\right)d\vec{\sigma}. \quad (40)$$

In the first integral the integration is performed over the volume of the cavity, V, while the second integral is taken over the boundary of the cavity, B. ν is the coordinate normal to the cavity boundary and J represents the current through the boundary. For the TM polarization, it equals the current at infinity.

From Eqs. (28) and (34) it follows that the field outside the cavity in the first order of the perturbative expansion is

$$\Psi_2(r,\theta) = \frac{H_m^{(1)}(kr)}{H_m^{(1)}(x)}\cos(m\theta) + \lambda(n^2-1)x_0 \times\sum_{p\neq m}A_{pm}\frac{H_p^{(1)}(kr)}{S_pH_p^{(1)}}\cos(p\theta).$$

The first order term proportional to $\cos(m\theta)$ is taken into account by calculating $H_m^{(1)}(x)$ instead of $H_m^{(1)}(x_0)$. The current can be directly calculated from Eq. (36) or from the asymptotic of the Hankel functions. Then the current can be written, neglecting first order variation for the $\cos(m\theta)$ term:

$$J = 4i\left[\frac{1}{|H_m^{(1)}|^2} + \lambda^2(n^2-1)^2 x_0^2 \sum_{p\neq m} \frac{A_{pm}^2}{|S_p H_m^{(1)}|^2}\right]. \tag{41}$$

To calculate the integral over the cavity volume in the leading order, the nonperturbed function can be used inside the cavity. Then the integration over the circle $r=R$ leads to

$$\int_V |\Psi(\vec{x})|^2 d\vec{x} \approx \frac{\pi}{J_m^2(nx_0)} \int_0^R J_m^2(nkr) r\, dr. \tag{42}$$

The last integral is (see [7], 7.14.1)

$$\int_0^R J_m^2(nkr) r\, dr = \frac{R^2}{2}\left[J_m'^2(nkR) + J_m^2(nkR)\left(1 - \frac{m^2}{(nkR)^2}\right)\right].$$

From the eigenvalue equation (10) and the asymptotic (15), it follows that

$$n\frac{J_m'(nkR)}{J_m(nkR)} \approx -\sqrt{m^2/x^2 - 1}.$$

Therefore,

$$\int_0^R J_m^2(nkr) r\, dr \approx J_m^2(nx_0)\frac{(n^2-1)R^2}{2n^2}. \tag{43}$$

Combining these equations leads to

$$\operatorname{Im} x = -\frac{2}{\pi}\left[\frac{1}{(n^2-1)x_0|H_m^{(1)}|^2} + \lambda^2(n^2-1)x_0 \sum_{p\neq m} \frac{A_{pm}^2}{|S_p H_m^{(1)}|^2}\right]. \tag{44}$$

According to Eq. (17) the first term of this expression is the imaginary part of the unperturbed quasistationary eigenvalue [assuming that $\operatorname{Im}(x_0) \ll \operatorname{Re}(x_0)$] and one gets Eq. (37) using only the first order corrections. The missing terms are proportional to the imaginary part of the unperturbed level and can safely be neglected for the well confined levels.

These calculations clearly demonstrate that the deformation of the cavity leads to the scattering of the initial well confined wave function with $\operatorname{Re}(kR) < m < n\operatorname{Re}(kR)$ into all possible states with different p momenta. Among these states, some are very little confined or not confined at all. These states with $p < \operatorname{Re}(kR)$ give the dominant contribution to the lifetime of perturbation eigenstates. Such scattering picture becomes more clear in the Green function approach discussed in Sec. III B.

The important quantity for applications is the far-field emission. It is calculated using the coefficients a_p (34) and b_p (35) in Eq. (28) and substituting its asymptotic for $H_p^{(1)}(kr)$:

$$H_p^{(1)}(kr) \xrightarrow{r\to\infty} \sqrt{\frac{2}{\pi kr}} e^{i(kr - \pi p/2 - \pi/4)}. \tag{45}$$

Then one gets

$$\Psi_2(r,\theta) \xrightarrow{r\to\infty} \sqrt{\frac{2}{\pi kr}} e^{i(kr-\pi/4)} F(\theta), \tag{46}$$

where

$$F(\theta) = (1+b_m)\frac{e^{-i\pi m/2}}{H_m^{(1)}(x)}\cos(m\theta) + \sum_{p\neq m}(a_p + b_p)\frac{e^{-i\pi p/2}}{H_p^{(1)}(x)}\cos(p\theta). \tag{47}$$

The boundary shift method discussed in this section is a simple and straightforward approach to perturbation series expansions for dielectric cavities. As it is based on Eqs. (23)–(26), it first shrinks to zero the regions where the refractive index differs from its value for the circular cavity. Consequently, the calculation of the field distribution in these regions remains unclear. Besides the direct continuation of perturbation series (34) inside these regions diverges. To clarify this point, we discuss in the next section a different method without such a drawback.

B. Green function method

Fields in two-dimensional dielectric cavities obey the Helmholtz equations (2) which can be written as one equation in the whole space for TM polarization

$$[\Delta + k^2 n^2(\vec{x})]\Psi(\vec{x}) = 0 \tag{48}$$

with position dependent "potential" $n^2(\vec{x})$. For perturbed cavity (20)

$$n^2(\vec{x}) = n_0^2(\vec{x}) + \delta n^2(\vec{x}) \tag{49}$$

where $n_0^2(\vec{x})$ is the "potential" for the pure circular cavity

$$n_0^2(\vec{x}) = \begin{cases} n^2 & \text{when } |\vec{x}| < R \\ 1 & \text{when } |\vec{x}| > R, \end{cases} \tag{50}$$

and the perturbation $\delta n^2(\vec{x})$ is equal to

$$\begin{array}{ll} (n^2-1) & \text{when } f(\theta) > 0 \text{ and } R < |\vec{x}| < R + \lambda f(\theta), \\ -(n^2-1) & \text{when } f(\theta) < 0 \text{ and } R + \lambda f(\theta) < |\vec{x}| < R, \\ 0 & \text{in all other cases}. \end{array} \tag{51}$$

Hence the integral of $\delta n^2(\vec{x})$ with an arbitrary function $F(\vec{x}) \equiv F(r,\theta)$ can be calculated as follows:

$$\int \delta n^2(\vec{x}) F(\vec{x}) d\vec{x} = (n^2-1)\int d\theta \int_R^{R+\lambda f(\theta)} F(r,\theta) r\, dr. \tag{52}$$

Equation (48) with "potential" (49) can be rewritten in the form

$$[\Delta_{\vec{x}} + k^2 n_0^2(\vec{x})]\Psi(\vec{x}) = -k^2 \delta n^2(\vec{x})\Psi(\vec{x}). \tag{53}$$

Then its formal solution is given by the following integral equation

$$\Psi(\vec{x}) = -k^2 \int G(\vec{x},\vec{y})\delta n^2(\vec{y})\Psi(\vec{y}) d\vec{y}, \tag{54}$$

where $G(\vec{x},\vec{y})$ is the Green function of the equation for the dielectric circular cavity which describes the field produced at point $\vec{x}$ by the delta-function source situated at point $\vec{y}$. The explicit expressions of this function are presented in Appendix C.

It is convenient to divide the $\vec{x}$ plane into three circular regions $r<R_1$, $R_1<r<R_2$, and $r>R_2$ where

$$R_1 = \min_\theta[R, R+\lambda f(\theta)],$$

$$R_2 = \max_\theta[R, R+\lambda f(\theta)]. \tag{55}$$

The boundaries of these regions are indicated by dashed circles in Fig. 4. Notice that the deformation "potential" $\delta n^2(\vec{x})$ is nonzero only in the second region $R_1<r<R_2$. Due to singular character of the Green function (cf. Appendix C), wave functions inside each region are represented by different expressions.

Let (r,θ) be the polar coordinates of point $\vec{x}$. For simplicity we assume for a moment that $f(\theta)\leq 0$. Using Eq. (C10), Eq. (54) in the region $r<R_1$ can be rewritten in the form

$$\Psi(\vec{x}) = \sum_p \frac{J_p(nkr)}{J_p(nx)}\cos(p\theta)\hat{L}_p[\Psi], \tag{56}$$

where $\hat{L}_p[\Psi]$ is the following integral operator:

$$\begin{aligned}\hat{L}_p[\Psi] = {}& \frac{x^2(n^2-1)}{R^2}\int d\phi\cos(p\phi)\\ &\times\int_R^{R+\lambda f(\phi)}\rho\, d\rho\Bigg[\frac{J_p(nk\rho)}{2\pi x S_p(x)J_p(nx)}\\ &+\frac{i}{4}[H_p^{(1)}(kn\rho)J_p(nx)-H_p^{(1)}(nx)J_p(kn\rho)]\Bigg]\\ &\times\Psi(\rho,\phi).\end{aligned} \tag{57}$$

Assuming that we are looking for corrections to a quasistationary state of the nonperturbed circular cavity with the momentum equal to m, one concludes that the quantized eigenenergies are fixed by the condition that the perturbation terms do not change zeroth order function (see, e.g., [14]), i.e.,

$$\hat{L}_m[\Psi] = 1 \tag{58}$$

which can be transformed into

$$\begin{aligned}S_m(x) = {}& \frac{x^2(n^2-1)}{R^2}\int d\phi\cos(p\phi)\\ &\times\int_R^{R+\lambda f(\phi)}\Psi(\rho,\phi)\rho\, d\rho\Bigg[\frac{J_m(nk\rho)}{2\pi x J_m(nx)}+\frac{iS_m(x)}{4}\\ &\times[H_m^{(1)}(kn\rho)J_m(nx)-H_m^{(1)}(nx)J_m(kn\rho)]\Bigg].\end{aligned} \tag{59}$$

To perform the perturbation iteration of Eqs. (56) and (59), integrals like the following must be calculated:

$$V_{pm} \equiv \frac{1}{J_m(nx)}\hat{L}_p[J_m(kn\rho)\cos(m\phi)]. \tag{60}$$

For small λ the integral over ρ can be computed by expanding the integrand into a series of $\delta r=\rho-R$,

$$\int_R^{R+\lambda f(\phi)} F(\rho)d\rho \approx \lambda f(\phi)F(R)+\frac{1}{2}\lambda^2 f^2(\phi)F'(R)+\cdots. \tag{61}$$

Notice that this method is valid only outside the second region $R_1<r<R_2$ which shrinks to zero when $\lambda\to 0$ [cf. Eq. (55)]. In such a manner, it leads to

$$V_{pm} = x^2(n^2-1)(\lambda V_{pm}^{(1)}+\lambda^2 V_{pm}^{(2)}), \tag{62}$$

where

$$V_{pm}^{(1)} = \frac{1}{xS_p(x)}A_{pm} \tag{63}$$

and

$$V_{pm}^{(2)} = \frac{B_{pm}}{2xS_p(x)}\left[1+x\left(\frac{H_p^{(1)\prime}(x)}{H_p^{(1)}(x)}+\frac{H_m^{(1)\prime}(x)}{H_m^{(1)}(x)}\right)-2xS_m(x)\right]. \tag{64}$$

Here A_{pm} and B_{pm} are defined in Eqs. (B5) and (B10).

The second order terms can also be expressed through V_{mp}:

$$\begin{aligned}\Psi(\vec{x}) = {}& \frac{J_m(knr)}{J_m(nx)}\cos(m\theta)+\sum_{p\neq m}\frac{J_p(knr)}{J_p(nx)}\cos(p\theta)\\ &\times\left[V_{pm}+\sum_{k\neq m}V_{pk}V_{km}\right].\end{aligned} \tag{65}$$

The quantization condition (58) in the second order states that

$$V_{mm}+\sum_{k\neq m}V_{mk}V_{km} = 1, \tag{66}$$

which can be expressed as

$$\begin{aligned}S_m(x) = {}& x(n^2-1)\left(\lambda A_{mm}+\frac{1}{2}\lambda^2\left[1+2x\frac{H_m^{(1)\prime}(x)}{H_m^{(1)}(x)}\right]B_{mm}\right)\\ &+\lambda^2 x^2(n^2-1)^2\sum_{k\neq m}\frac{A_{mk}A_{km}}{S_k(x)}.\end{aligned} \tag{67}$$

Writing as in the previous section $x=x_0+\lambda x_1+\lambda^2 x_2$ where x_0 is a zero of $S_m(x)$ and using Eq. (B1), one obtains the same series as Eq. (33). Other expansions up to the second order also coincide with the ones presented in Sec. III A.

To calculate the higher terms of the perturbation expansion, the wave function must be known in the regions where the perturbation "potential" $\delta n^2(\vec{x})$ is nonzero. But exactly in these regions the Green function differs from the one used in Eq. (57). In other words, a method must be found for the continuation of the wave functions defined in the first region $r<R_1$ (or in the third one $r>R_2$) into the second region $R_1<r<R_2$.

The straightforward way of such a continuation is to use explicit formulas for the Green function in the second region and to perform the necessary calculations. As the radial derivative of the Green function is discontinuous, delta-function contributions will appear in certain domains when calculating the integrals as in Eq. (61). One can check that this singular contribution appears in the bulk only in the third order in λ in agreement with Eqs. (33) and (34).

The expansion of wave functions into series of the Bessel functions (56), in general, diverges when $r>R_1$ and the Green function method gives the correct continuation inside this region. Another equivalent method consists in a local expansion of wave function into power series in small deviation from the boundary of convergence. As the value of the function and its radial derivative are assumed to be known along this boundary ($r=R_1$ in our case) the knowledge of the wave equation inside and outside the cavity determines uniquely the wave function in the both regions.

IV. APPLICABILITY OF PERTURBATION SERIES

In the previous section the formal construction of perturbation series has been performed for quasibound states in slightly deformed dielectric cavities. The purpose of this section is to discuss in detail the conditions of validity of such an expansion.

From Eq. (B5) it follows that the coefficients A_{pm} obey the inequality

$$|A_{pm}| \leqslant 2\xi, \tag{68}$$

where ξ stands for

$$\xi = \int \left|\frac{f(\theta)}{R}\right| d\theta \approx \frac{\delta a}{\pi R^2}. \tag{69}$$

Here δa is the surface where the perturbation "potential" δn^2 is nonzero and πR^2 is the full area of the unperturbed circle. The last equality is valid when Eq. (21) is fulfilled which we always assume.

Consequently, the perturbation formulas can be applied providing

$$\xi(n^2-1)u\left\langle \left|\frac{1}{S_p(u)}\right| \right\rangle \ll 1, \tag{70}$$

where $\langle F_p \rangle$ indicates the typical value of F_p and u stands for $\mathrm{Re}(kR)$ at a first approximation.

The usual arguments to estimate this quantity for large x_0 are the following. In the strict semiclassical approximation, states with a corresponding incident angle larger than the critical angle have a very small imaginary part and are practically true bound states. For closed circular cavities, the mean number of states (counting doublets only once) is given by the Weyl law

$$N(E_j < n^2k^2) = \frac{An^2}{8\pi}k^2 + O(k), \tag{71}$$

where $A=\pi R^2$ is the full billiard area and n is the refractive index. The latter appears because by definition inside the cavity the energy is $E=n^2k^2$. For a dielectric circular cavity with radius R, the condition that the incidence angle is larger than the critical angle leads to the following effective area [12]

$$A_{\mathrm{eff}}(n) = \pi R^2 s_n, \tag{72}$$

where

$$s_n = \frac{2}{R^2}\int_{R/n}^{R}\left(1-\frac{2}{\pi}\arcsin\frac{R}{nr}\right) r\,dr \tag{73}$$

$$= \frac{4}{\pi n^2 x}\int_x^{nx}\sqrt{x^2n^2-m^2}\,dm$$

$$= 1-\frac{2}{\pi}\left(\arcsin\frac{1}{n}+\frac{1}{n}\sqrt{1-\frac{1}{n^2}}\right). \tag{74}$$

Here the first integral (73) corresponds to the straightforward calculation of phase-space volume such that the incident angle is larger than the critical one and the second integral (74) is obtained from Eq. (16) taking into account that $x<m<nx$. For $n=1.5$, $s_n \approx 0.22$.

Consequently, the typical distance between two eigenstates is

$$\delta x \sim \frac{4}{n^2 s_n x}. \tag{75}$$

The eigenmomenta of nonconfining eigenstates have imaginary parts of the order of unity [cf. Eq. (13)] and will be ignored.

As $S_m(x_0)=0$, we estimate that for $p\neq m$

$$\left\langle \frac{1}{S_p} \right\rangle \sim \left|\frac{1}{S'\,\delta x}\right|. \tag{76}$$

Using Eq. (B1) one finds that this value is of the order of

$$\left\langle \frac{1}{S_p} \right\rangle \sim Cx, \tag{77}$$

where constant $C \sim 0.25n^2 s_n/(n^2-1)$. With Eq. (70) it leads to the conclusion that for typical S_p the criterion of applicability of perturbation series is

$$s_n\frac{\delta a}{8\pi}k^2n^2 \ll 1, \tag{78}$$

which up to a numerical factor agrees with Eq. (22).

But this statement is valid only in the mean. If there exist quasi-degeneracies of the nonperturbed spectrum [i.e., there exist p for which $1/S_p(x)$ is considerably larger than the estimate (77)] then the standard perturbation treatment requires modifications. As circular cavities are integrable, the real parts of the strongly confined modes are statistically distributed as the Poisson sequences [15] and they do have a large number of quasidegeneracies even for small k. For instance, these are double quasicoincidences for the dielectric circular cavity with $n=1.5$,

$$x_{14,2} = 16.7170 - 0.03895i, \quad x_{11,4} = 16.6976 - 0.4695i,$$

$$x_{15,3} = 17.5042 - 0.37540i, \quad x_{12,4} = 17.5232 - 0.4612i,$$

$$x_{17,4} = 21.5715 - 0.41621i, \quad x_{14,5} = 21.5106 - 0.4712i,$$

$$x_{25,1} = 19.4799 - 0.00254i, \quad x_{21,2} = 19.4830 - 0.1211i.$$

We notice also a triple quasicoincidence

$$x_{46,1} = 34.3110 - 2.2206 \times 10^{-6}i,$$

$$x_{41,2} = 34.3167 - 0.001982i,$$

$$x_{37,3} = 34.317 - 0.06408i. \tag{79}$$

The existence of these quasidegeneracies means that the perturbation series require modifications close to these values of kR for any small deformations of a circular cavity with $n=1.5$.

Double quasidegeneracy is the simplest case because there is only one eigenvalue of the dielectric circle, with quantum number, say p, whose eigenvalue is close to the eigenvalue x_0 corresponding to the quantum number m. In such a situation, instead of the zeroth order equation (31), the system of the following two equations must be considered

$$S_m[x_0(1+\delta x)]a_1 = M_{11}a_1 + M_{12}a_2,$$

$$S_p[x_0(1+\delta x)]a_2 = M_{21}a_1 + M_{22}a_2, \tag{80}$$

where in the leading order $M_{ij}=x_0(n^2-1)A_{ij}$.

Expanding the S_p functions and using the dominant order (B1) for S'_p, the system (80) can be transformed into

$$(s_1 - \delta x)a_1 = A_{12}a_2,$$

$$(s_2 - \delta x)a_2 = A_{21}a_1 \tag{81}$$

where

$$s_1 = \frac{S_m(x_0)}{x_0(n^2-1)} - A_{11}, \quad s_2 = \frac{S_p(x_0)}{x_0(n^2-1)} - A_{22}. \tag{82}$$

Our usual choice is $S_m(x_0)=0$ but for symmetry we do not impose it. The compatibility of the system (81) leads to the equation

$$\begin{vmatrix} \delta x - s_1 & A_{12} \\ A_{21} & \delta x - s_2 \end{vmatrix} = 0. \tag{83}$$

Its solution which tends to s_1 when $A_{12}A_{21} \to 0$ is

$$\delta x = \frac{1}{2}(s_1+s_2) + \frac{1}{2}(s_1-s_2)\sqrt{1+\frac{4A_{12}A_{21}}{(s_1-s_2)^2}}$$

$$= s_1 - \frac{A_{12}A_{21}}{s_2-s_1}\frac{2}{1+\sqrt{1+4A_{12}A_{21}/(s_1-s_2)^2}}. \tag{84}$$

When $A_{12}A_{21}/(s_1-s_2)^2$ is small, δx in Eq. (84) tends to the usual contribution of the second order (33). Therefore, in this approximation, expression (33) may be used for all p except the one which is quasidegenerate with x_0. For this later one, the whole expression (84) (without s_1) has to be used. A useful approximation proposed in [16] consists in taking the modification (84) for all the nondegenerate levels which reduces the numerical calculations.

As the circular billiard is integrable, the probability of having three and more quasidegeneracies is not negligible [cf. Eq. (79)]. The necessary modifications can be performed for any number of levels but the resulting formulas become cumbersome. In Appendix D we present the formulas for three quasidegenerate levels.

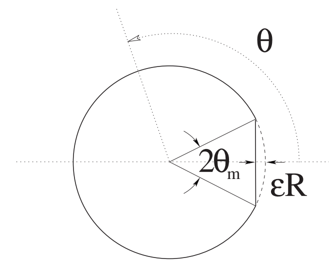

FIG. 5. Cut disk cavity. ϵR is the distance between the cut and the circular boundary.

V. CUT DISK

As a specific example, we consider a deformation of the circular cavity which is useful for experimental and technological points of view [17]. Namely, a circle is cut over a straight line (see Fig. 5). Such a deformation is characterized by the parameter $\epsilon \ll 1$ which determines the distance from the cut to the circular boundary. This shape corresponds to the following choice of the deformation function $f(\theta)$

$$f(\theta) = R\left(1 - \frac{1-\epsilon}{\cos\theta}\right) \approx R\left(\epsilon - \frac{\theta^2}{2} + \frac{\epsilon\theta^2}{2} - \frac{5\theta^4}{24}\right), \tag{85}$$

when $|\theta| < \theta_m$ and $f(\theta)=0$ for other values of θ. Here θ_m is the small angle

$$\theta_m = \arccos(1-\epsilon) \simeq \sqrt{2\epsilon} + \frac{\sqrt{2}}{12}\epsilon^{3/2}. \tag{86}$$

Using the formulas discussed in the preceding sections, we compute all the necessary quantities and compare them with the results of the direct numerical simulations based on a boundary element representation similar to the one discussed in [13].

The spectrum of quasi-bound states for a cut disk with $\epsilon=0.05$ is plotted in Fig. 6. To get a good agreement in the region $\mathrm{Re}(kR) \simeq 15-20$, it is necessary to take into account double quasidegeneracies and, in the region close to $\mathrm{Re}(kR)=35$, triple degeneracy (79) has been considered. The agreement is quite good even in the region of large kR where many families intersect.

Two wave functions of this cut disk are plotted in Fig. 7. The first one is obtained by direct numerical simulations and the second one corresponds to the perturbation expansion. Even tiny details are well reproduced by perturbation computations. In the direct numerical simulations, the wave functions are reconstructed from the knowledge of the boundary currents. This procedure requires the integration of the Han-

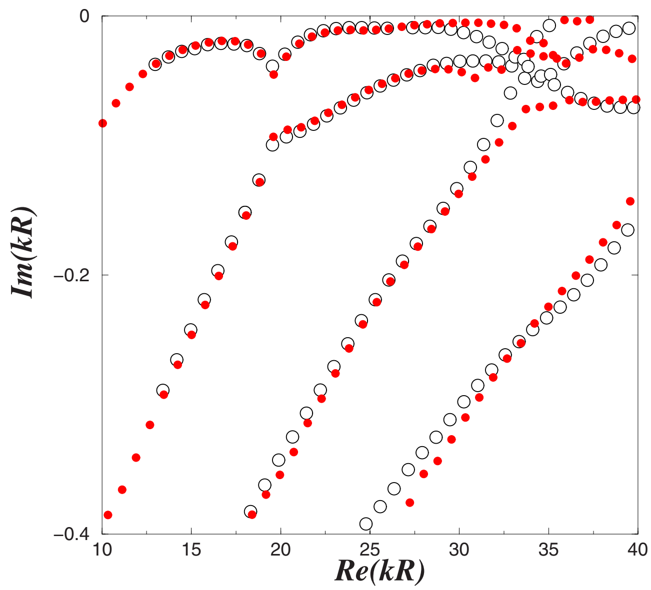

FIG. 6. (Color online) Comparison between perturbation and numerical spectra for the cut disk with $\epsilon=0.05$. Open circles are results of the direct numerical simulations and full circles correspond to the perturbation expansion (33).

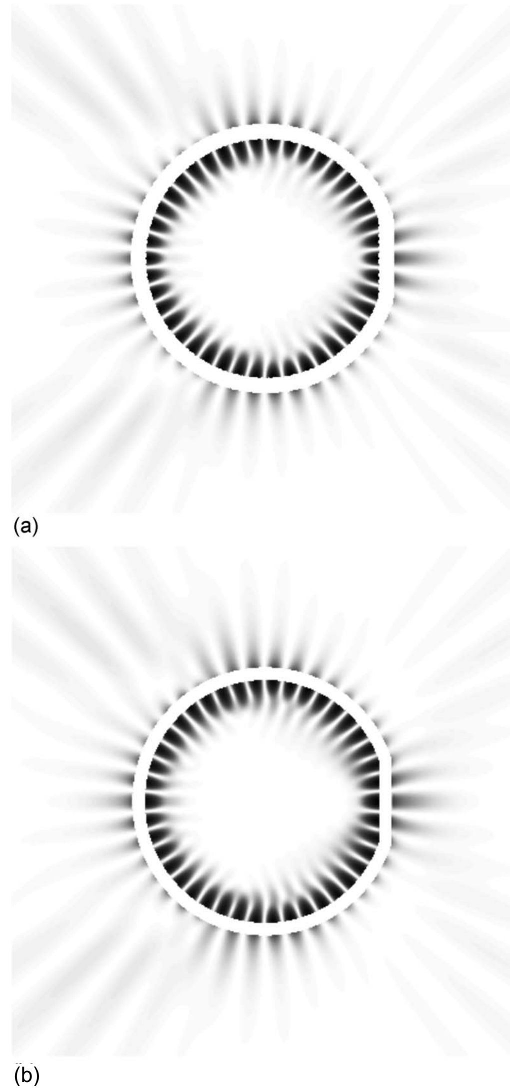

FIG. 7. (a) Modulus square of the wave function for the cut disk with $\epsilon=0.05$ obtained by direct numerical simulations corresponding to quasistationary eigenmomentum $kR=16.655-0.0199i$. (b) The same but calculated within perturbation expansion with $m=21$ and $p=0$. The corresponding eigenmomentum is $kR=16.659-0.0191i$. The high intensity regions are indicated in black.

kel function, $H_0^{(1)}$ [13]. As this function has a logarithmic singularity, a small region around the cavity boundary has been removed to reduce numerical errors. It explains the white region in Fig. 7(a). For an easier comparison, the same region has been removed also from the perturbation result in Fig. 7(b).

Finally, in Fig. 8, the far-field emission pattern computed numerically for the cut disk is compared with the same deduced from the perturbation series (47). Both are normalized to unit maximum. Once more a good agreement is found. The approximate positions of the main peaks in the far-field pattern correspond to the diffracted rays emanated from the discontinuities of the cut disk boundaries and reflected at the critical angle (8) on the circular boundary (see Fig. 9). If $(\theta_1,\theta_2,\ldots)$ and $(\theta_1',\theta_2',\ldots)$ are the directions of two such refracted rays one gets from geometrical considerations

$$\theta_1=\frac{\pi}{2}+2\theta_c-\theta_m,\quad \theta_1'=\frac{3\pi}{2}-2\theta_c-\theta_m,$$

$$\theta_2=4\theta_c-\theta_m-\frac{\pi}{2},\quad \theta_2'=4\theta_c+\theta_m-\frac{\pi}{2}. \qquad (87)$$

Here θ_c is the critical angle (8) and θ_m is defined in Eq. (86). For $\epsilon=0.05$ and $n=1.5$, $\theta_1\approx 155.4°$, $\theta_1'\approx 168.2°$, $\theta_2\approx 59°$, and $\theta_2'\approx 95.4°$ which agrees with Fig. 8.

To complete this study, far-field experiments have been carried out according to the set-up described in [18]. The cavities are made of a layer of polymethylmethacrylate (PMMA) doped by 4-*dicyanomethylene*-2-*methyl*-6-(4-*dimethylaminostyryl*)-4*H*-*pyran* (DCM, 5% in weight) on a silica on silicon wafer. To obtain a good resolution of the shape even for such a small cut as $\epsilon=0.05$, cavities are defined with electron beam lithography (Leica EBPG 5000+) by C. Ulysse (Laboratoire de Photonique et de Nanostructures, CNRS-UPR20). A scanning electron microscope image of such a cavity is shown in Fig. 10. As specified in [18], the cavities are uniformly pumped one by one from the top at 532 nm with a pulsed doubled Nd:YAG laser. The light emitted from the cavity is collected in its plane with a lens leading to a 10° apex angle aperture. The directions of emission are symmetrical about the 0° axis according to the obvious symmetry of the cut-disk shape. In Fig. 8, the intensity detected in the far field is plotted versus the θ angle with points. The position of the maximal peak around 160° is reproducible from cavity to cavity with $\epsilon=0.05$ and agrees with both numerical and perturbation approaches.

The example of the cut disk clearly demonstrates the usefulness of the perturbation method presented in this paper for deformed circular cavities.

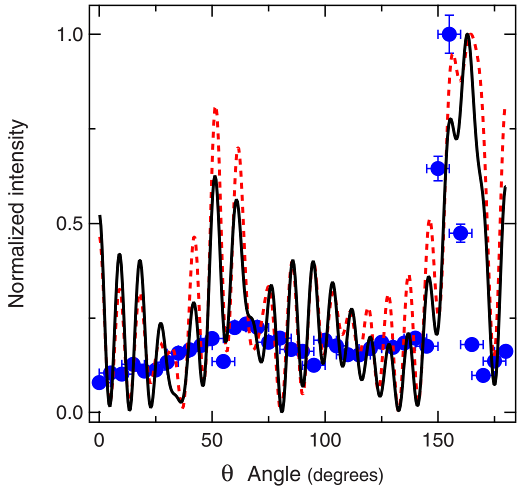

FIG. 8. (Color online) Far-field emission pattern, $|F(\theta)|^2$, for the same state as in Fig. 7. Results from direct numerical simulations are plotted in solid line, while the dashed line indicates the perturbation result (47). The points correspond to experimental results with $\epsilon=0.05$ and $R=60$ μm.

VI. CONCLUSION

We considered in detail the construction of perturbation series for deformed dielectric circular cavities. The obtained formulas can be applied for the calculation of the spectrum and the wave functions as well as other characteristics of these dielectric cavities (e.g., far-field emission patterns). We checked these formulas on the example of the cut disk which is of interest from an experimental point of view. Cavities of other shapes (e.g., spiral [19]) can be considered analogously. This method can also be used to calculate the influence of a small boundary roughness on the emission properties of circular cavities.

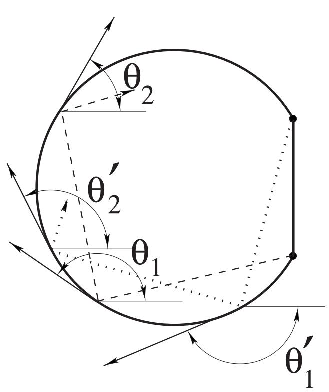

FIG. 9. Dashed and dotted lines: Two main diffracted rays responsible for dominant peaks in the far-field pattern of a dielectric cut disk. All rays hit the circular boundary with an angle equal the critical angle (8).

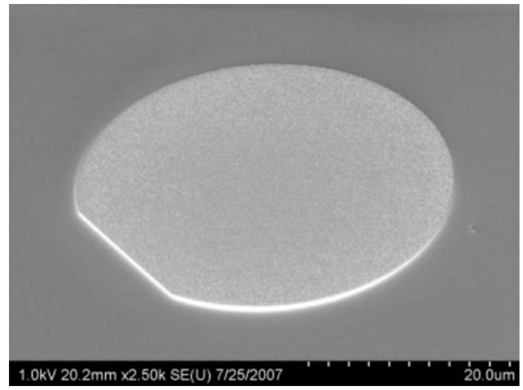

FIG. 10. Scanning electron microscope image of a cut disk etched with an electron beam.

ACKNOWLEDGMENTS

The authors are grateful to J.-S. Lauret and J. Zyss for fruitful discussions, to D. Bouche for pointing out Ref. [11], to H. Schomerus for pointing out Ref. [9], and to G. Faini and C. Ulysse (Laboratoire de Photonique et de Nanostructures, CNRS-UPR20) for technical support.

APPENDIX A: WHISPERING GALLERY MODES

The purpose of this appendix is to calculate the asymptotic of quasistationary eigenvalues for a fixed radial quantum number p and a large azimuthal quantum number $m\to\infty$.

These resonances are well confined, so let us first find the corresponding asymptotic expression for zeros of Bessel functions $J_m(x_m)=0$. To achieve this task it is convenient to use Langer's formulas (see, e.g., [7], 7.13.4) which are valid with $O(m^{-4/3})$ accuracy

$$J_m(x) = T(w)[J_{1/3}(z)\cos(\pi/6) - Y_{1/3}(z)\sin(\pi/6)],$$

$$Y_m(x) = T(w)[J_{1/3}(z)\cos(\pi/6) + Y_{1/3}(z)\sin(\pi/6)],$$

where $T(w)=w^{-1/2}[w-\arctan(w)]^{1/2}$, $w=(x^2/m^2-1)^{1/2}$, and $z=m[w-\arctan(w)]$.

The combination of the Bessel functions is expressed as follows

$$J_{1/3}(z)\cos(\pi/6) - Y_{1/3}(z)\sin(\pi/6) = 3^{1/6}2^{1/3}z^{-1/3}\mathrm{Ai}[-(3z/2)^{2/3}], \tag{A1}$$

where Ai(x) is the Airy function

$$\mathrm{Ai}(x) = \frac{1}{\pi}\int_0^\infty \cos\left(\frac{t^3}{3}+tx\right)dt. \tag{A2}$$

Therefore, in the intermediate region when z is fixed and $m \gg 1$, the zeros of the J_m Bessel function correspond to

$$z = \frac{2}{3}\eta_p^{3/2}, \tag{A3}$$

where η_p are the modulus of the zeros of the Airy function $\mathrm{Ai}(-\eta_p)=0$ ($\eta_1\approx 2.338$, $\eta_2\approx 4.088$, and $\eta_3\approx 5.521$). Finally, the Bessel function zeros have the following expansion

$$x_m = m + \alpha m^{1/3} + \beta m^{-1/3} + O(m^{-1}), \tag{A4}$$

where

$$\alpha = 2^{-1/3}\eta_p, \quad \beta = \frac{3}{2^{5/3}5}\eta_p^2. \tag{A5}$$

For $p=1$ this expression agrees numerically with the one given in [7], Sec. 7.9.

The whispering gallery zeros of Bessel functions (A4) permit us to calculate explicitly the whispering gallery modes for the dielectric disk. Indeed we are interested in the solutions of equation

$$\frac{n}{\nu}\frac{J_m'}{J_m}(nx) = \frac{H_m^{(1)\prime}}{H_m}(x) \tag{A6}$$

in the region xn close to m, which means

$$xn = x_m + \delta x \tag{A7}$$

with $\delta x \ll x_m$. The expansion of the right-hand side of Eq. (A6) leads to

$$\frac{H_m^{(1)\prime}}{H_m}\left(\frac{x_m}{n}\right) = -\sqrt{n^2-1} + \frac{\alpha n^2}{m^{2/3}\sqrt{n^2-1}} + O(m^{-1}). \tag{A8}$$

In the left-hand side of Eq. (A6), both numerator and denominator can be expanded into powers of δx taking into account that $J_m(x_m)=0$

$$\frac{J_m'}{J_m}(x_m+\delta x) \approx \frac{J_m' + \delta x J_m'' + (\delta x)^2 J_m'''}{\delta x J_m' + (\delta x)^2 J_m''/2 + (\delta x)^3 J_m'''/6}(x_m). \tag{A9}$$

Using the Bessel equation

$$J_m''(z) + \frac{1}{z}J_m'(z) + \left(1 - \frac{m^2}{z^2}\right)J_m(z) = 0 \tag{A10}$$

one can check that all but one derivatives $J_m^{(k)}/J_m'(x_m)$ are at most $O(m^{-1})$ and can be neglected. The only exception is

$$\frac{J_m'''}{J_m'}(x_m) = -\frac{2\alpha}{m^{2/3}} + O(m^{-1}). \tag{A11}$$

Finally, expansion (A9) takes the form

$$\frac{J_m'}{J_m}(x_m+\delta x) = \frac{1}{\delta x} - \delta x\frac{2\alpha}{3m^{2/3}} + O(m^{-1}). \tag{A12}$$

Combining this equation with Eqs. (A6) and (A8) one obtains

$$\delta x = -\frac{n}{\nu\sqrt{n^2-1}} + \frac{\alpha n^3}{m^{2/3}\nu(n^2-1)^{3/2}}\left(\frac{2}{3\nu^2} - 1\right) + O(m^{-1}). \tag{A13}$$

These formulas lead to Eq. (18).

Other "whispering gallery" modes correspond to x close to m. With the same notations as above, Langer's formula can be written for the Hankel function

$$H_m^{(1)}(x) = T(w)e^{i\pi/6}H_{1/3}^{(1)}(z) + O(m^{-4/3}). \tag{A14}$$

The zeros of $H_{1/3}(z)$ exist only when $z=re^{-i\pi}$ with real r. From formula [7] 7.11.42, it follows that

$$H_\nu^{(1)}(re^{im\pi}) = -\frac{\sin \pi(m-1)\nu}{\sin \pi\nu}H_\nu^{(1)}(r) + e^{-i\pi\nu}\frac{\sin \pi m\nu}{\sin \pi\nu}H_\nu^{(2)}(r). \tag{A15}$$

In this way, we get

$$H_{1/3}^{(1)}(re^{-i\pi}) = 2e^{-i\pi/6}[J_{1/3}(r)\cos(\pi/6) - Y_{1/3}(r)\sin(\pi/6)]. \tag{A16}$$

This is the same combination of the Bessel functions as Eq. (A1) for $J_m(x)$. Therefore, the first complex zeros of the Hankel function, $H_m^{(1)}(\tilde{x}_m)$, have a form similar to Eq. (A4)

$$\tilde{x}_m = m + \tilde{\alpha} m^{1/3} + \tilde{\beta} m^{-1/3} + O(m^{-1}), \tag{A17}$$

where $\tilde{\alpha}=e^{-2\pi i/3}\alpha$ and $\tilde{\beta}=e^{-4\pi i/3}\beta$ with the same α and β as in Eq. (A5).

The next step is to find the asymptotic of $J_m(nx)$ for complex $x=\tilde{x}_m$. As

$$Im(\tilde{x}_m) = -2^{-1/3}\sin(2\pi/3)\eta_p m^{1/3} + O(m^{-1/3}), \tag{A18}$$

it tends to $-\infty$ with increasing of m. Therefore, from Eq. (14) it follows that, instead of the $\cos(\cdots)$ term, only the positive exponent has to be taken into account. Then the left-hand side of Eq. (A6) leads to

$$\begin{aligned}\frac{J_m'}{J_m}(n\tilde{x}_m) &= i\sqrt{1 - \frac{m^2}{n^2\tilde{x}_m^2}} + O(m^{-1}) \\ &= i\frac{\sqrt{n^2-1}}{n}\left(1 + \frac{\tilde{\alpha}}{(n^2-1)m^{2/3}}\right) + O(m^{-1}).\end{aligned} \tag{A19}$$

As $H_m^{(1)}(z)$ also obeys Eq. (A10) one obtains the same expansion as Eq. (A12)

$$\frac{H_m^{(1)\prime}}{H_m^{(1)}}(\tilde{x}_m+\delta x) = \frac{1}{\delta x} - \delta x\frac{2\tilde{\alpha}}{3m^{2/3}} + O(m^{-1}). \tag{A20}$$

Equations (A19) and (A20) lead to the following value of δx with $O(m^{-1})$ accuracy

$$\delta x = -\frac{i\nu}{\sqrt{n^2-1}} + \frac{i\nu\tilde{\alpha}}{m^{2/3}\sqrt{n^2-1}}\left(1 - \frac{2\nu^2}{3}\right). \tag{A21}$$

Collecting these equations we get Eq. (19).

APPENDIX B: CONSTRUCTION OF PERTURBATION SERIES

From Eqs. (24)–(28), the following relations are valid at the circle $r=R$:

$$\Psi_1 - \Psi_2 = -\lambda^2\sum_p \gamma_p \cos(p\theta) + O(\lambda^3),$$

$$\frac{\partial\Psi_1}{\partial r}-\frac{\partial\Psi_2}{\partial r}=k\Bigg[S_m(x)\cos(m\theta)+\lambda\sum_{p\neq m}(\alpha_p+\lambda\beta_p)\times S_p(x)\cos(p\theta)+\lambda^2\sum_p\gamma_p\frac{H_p^{(1)\prime}}{H_p^{(1)}}(x_0)\times\cos(p\theta)\Bigg]+O(\lambda^3),$$

$$\frac{\partial^2\Psi_1}{\partial r^2}-\frac{\partial^2\Psi_2}{\partial r^2}=-\frac{k}{R}\Bigg([S_m(x)+x(n^2-1)]\cos(m\theta)+\lambda\sum_{p\neq m}\alpha_p[S_p(x_0)+x_0(n^2-1)]\cos(p\theta)\Bigg)+O(\lambda^2),$$

and

$$\frac{\partial^3\Psi_1}{\partial r^3}-\frac{\partial^3\Psi_2}{\partial r^3}=\Bigg[kS_m(x_0)\left(\frac{m^2+2}{R^2}-k^2n^2\right)-k^3(n^2-1)\times\frac{H_m^{(1)\prime}}{H_m^{(1)}}(x_0)+k^2\frac{n^2-1}{R}\Bigg]\cos(m\theta)+O(\lambda).$$

In the zeroth order $S_m(x_0)=0$. Expanding $S_m(x)$ with x as in Eq. (30) into a series in λ, one gets

$$S_m(x_0+\lambda x_1+\lambda^2x_2)=\lambda x_1\frac{\partial S_m}{\partial x}+\lambda^2\left(x_2\frac{\partial S_m}{\partial x}+\frac{1}{2}x_1^2\frac{\partial^2 S_m}{\partial x^2}\right)+O(\lambda^2),$$

where all derivatives of S_m are taken at $x=x_0$. These derivatives are deduced from the Bessel equation (A10)

$$\frac{\partial S_m}{\partial x}(x)=-(n^2-1)-\frac{1}{x}S_m(x)-S_m(x)\left(S_m(x)+2\frac{H_m^{(1)\prime}}{H_m^{(1)}}(x)\right).$$

In particular, when $x=x_0$,

$$\frac{\partial S_m}{\partial x}(x_0)=-(n^2-1),$$

$$\frac{\partial^2 S_m}{\partial x^2}(x_0)=(n^2-1)\left(\frac{1}{x_0}+2\frac{H_m^{(1)\prime}}{H_m^{(1)}}(x_0)\right). \tag{B1}$$

In the λ first order, it leads to

$$-x_1(n^2-1)\cos(m\theta)+\sum_{p\neq m}\alpha_pS_p(x_0)\cos(p\theta)=\frac{f(\theta)}{R}x_0(n^2-1)\cos(m\theta). \tag{B2}$$

Coefficients α_p and the first eigenvalue correction, x_1, are determined by comparison of the Fourier harmonics in both sides of Eq. (B2)

$$\alpha_p=(n^2-1)\frac{x_0}{S_p(x_0)}A_{pm} \tag{B3}$$

and

$$x_1=-x_0A_{mm}, \tag{B4}$$

where A_{pm} are the Fourier harmonics of the deformation function

$$A_{pm}=\frac{\epsilon_p}{\pi R}\int_0^\pi f(\theta)\cos(p\theta)\cos(m\theta)d\theta. \tag{B5}$$

Here

$$\epsilon_p=\begin{cases}2 & \text{for } p\neq 0\\ 1 & \text{for } p=0.\end{cases} \tag{B6}$$

In the λ second order, it leads to the following two equations:

$$\sum_p\gamma_p\cos(p\theta)=\frac{1}{2}x_0^2(n^2-1)\frac{f^2(\theta)}{R^2}\cos(m\theta) \tag{B7}$$

and

$$\left\{(n^2-1)\left[-x_2+\frac{1}{2x_0}x_1^2\left(1+2x_0\frac{H_m^{(1)\prime}}{H_m^{(1)}}\right)\right]+\gamma_m\frac{H_m^{(1)\prime}}{H_m^{(1)}}\right\}\cos(m\theta)+\sum_{p\neq m}\left[x_1\alpha_p\frac{\partial S_p}{\partial x}+\beta_pS_p+\gamma_p\frac{H_p^{(1)\prime}}{H_p^{(1)}}\right]\cos(p\theta)$$
$$=\frac{f(\theta)}{R}\sum_{p\neq m}\alpha_p[S_p+x_0(n^2-1)]\cos(p\theta)-\frac{f^2(\theta)}{2R^2}x_0(n^2-1)\times\left(1-x_0\frac{H_m^{(1)\prime}}{H_m^{(1)}}\right)\cos(m\theta). \tag{B8}$$

Using Eq. (B2), the right-hand side of Eq. (B8) can be rewritten as

$$(n^2-1)\frac{f(\theta)}{R}\left(x_0\sum_{p\neq m}\alpha_p\cos(p\theta)+x_1\cos(m\theta)\right)+(n^2-1)\frac{f^2(\theta)}{2R^2}x_0\left(1+x_0\frac{H_m^{(1)\prime}}{H_m^{(1)}}\right)\cos(m\theta).$$

Unknown coefficients can be determined by equating the Fourier harmonics in both parts of Eqs. (B7) and (B8). From Eq. (B7) it follows that for all p

$$\gamma_p=\frac{1}{2}x_0^2(n^2-1)B_{pm}, \tag{B9}$$

where B_{pm} represents the Fourier harmonics of the square of the deformation function

$$B_{pm}=\frac{\epsilon_p}{\pi R^2}\int_0^\pi f^2(\theta)\cos(p\theta)\cos(m\theta)d\theta. \tag{B10}$$

For $p\neq m$ Eq. (B8) gives

$$\beta_pS_p+x_1\alpha_p\frac{\partial S_p}{\partial x}+\gamma_p\frac{H_p^{(1)\prime}}{H_p^{(1)}}=(n^2-1)\left[x_1A_{pm}+x_0\sum_{k\neq m}\alpha_kA_{pk}+\frac{1}{2}x_0\left(1+x_0\frac{H_m^{(1)\prime}}{H_m^{(1)}}\right)B_{pm}\right].$$

The mth harmonic of the same equation determines the second correction to the quasistationary eigenvalue

$$x_2 = \frac{1}{2x_0}x_1^2\left(1 + 2x_0\frac{H_m^{(1)\prime}}{H_m^{(1)}}\right) + \frac{\gamma_m H_m^{(1)\prime}}{(n^2-1)H_m^{(1)}} - \frac{1}{2}x_0\left(1 + x_0\frac{H_m^{(1)\prime}}{H_m^{(1)}}\right)B_{mm} - x_0\sum_{k\neq m}\alpha_k A_{mk} - x_1 A_{mm}.$$

Rearranging these equations and using the first order results and Eq. (B9), one gets

$$x_2 = x_0\left[\frac{1}{2}(3A_{mm}^2 - B_{mm}) + x_0\frac{H_m^{(1)\prime}}{H_m^{(1)}}(A_{mm}^2 - B_{mm}) - \sum_{k\neq m}\alpha_k A_{m,k}\right] \tag{B11}$$

and

$$\beta_p = x_0\frac{n^2-1}{S_p}\left\{A_{pm}A_{mm}\left(\frac{x_0}{S_p}\frac{\partial S_p}{\partial x} - 1\right) + \frac{1}{2}B_{pm}\left[1 + x_0\left(\frac{H_m^{(1)\prime}}{H_m^{(1)}} + \frac{H_p^{(1)\prime}}{H_p^{(1)}}\right)\right] + \sum_{k\neq m}\alpha_k A_{pk}\right\}. \tag{B12}$$

APPENDIX C: GREEN FUNCTION FOR THE DIELECTRIC CIRCULAR CAVITY

The Green function of the dielectric Helmholtz equation for the circular cavity, $G(\vec{x},\vec{y})$, is defined as the solution of the following equation

$$[\Delta_{\vec{x}} + n_0^2(\vec{x})k^2]G(\vec{x},\vec{y}) = \delta(\vec{x}-\vec{y}), \tag{C1}$$

where n_0^2 is the potential for the circular cavity defined in Eq. (50).

Let us first consider the case when the $\vec{y}$ source point is inside the circle. In this case, when the $\vec{x}$ point is inside the cavity, the advanced Green function has the form

$$G(\vec{x},\vec{y}) = \sum_{m=-\infty}^{\infty} A_m J_m(nkr)e^{im(\theta-\phi)} + \frac{1}{4i}H_0^{(1)}(kn|\vec{x}-\vec{y}|) \tag{C2}$$

and when the $\vec{x}$ point is outside the circle

$$G(\vec{x},\vec{y}) = \sum_{m=-\infty}^{\infty} B_m H_m^{(1)}(kr)e^{im(\theta-\phi)}. \tag{C3}$$

Here and below we assume that points $\vec{x}$ and $\vec{y}$ have polar coordinates (r,θ) and (ρ,ϕ), respectively.

Constants A_m and B_m are calculated from the boundary conditions on the interface using the expansion [7] 7.15.29 of $H_0^{(1)}(k|\vec{x}-\vec{y}|)$,

$$H_0^{(1)}(k|\vec{x}-\vec{y}|) = \sum_{m=-\infty}^{\infty} J_m(kr)H_m^{(1)}(k\rho)e^{im(\theta-\phi)} \tag{C4}$$

when $r<\rho$ and

$$H_0^{(1)}(k|\vec{x}-\vec{y}|) = \sum_{m=-\infty}^{\infty} H_m^{(1)}(kr)J_m(k\rho)e^{im(\theta-\phi)} \tag{C5}$$

when $r>\rho$.

For the TM polarization the Green function and its normal derivative at circle boundary are continuous. That leads to the following system of equations (with $x=kR$):

$$A_m J_m(nx) + \frac{1}{4i}J_m(nk\rho)H_m^{(1)}(nx) = B_m H_m^{(1)}(x),$$

$$nA_m J_m'(nx) + \frac{n}{4i}J_m(nk\rho)H_m^{(1)\prime}(nx) = B_m H_m^{(1)\prime}(x).$$

Its solutions are

$$A_m = -\frac{H_m^{(1)}(x)}{2\pi x\Delta_m J_m(nx)}J_m(kn\rho) - \frac{H_m^{(1)}(nx)}{4iJ_m(nx)}J_m(kn\rho),$$

$$B_m = -\frac{1}{2\pi x\Delta_m}J_m(kn\rho),$$

where

$$\Delta_m = nJ_m'(nx)H_m^{(1)}(x) - J_m(nx)H_m^{(1)\prime}(x) \equiv J_m(nx)H_m^{(1)}(x)S_m(x). \tag{C6}$$

In deriving these expressions, the Wronskian ([7], 7.11.29) has been used

$$J_\nu(x)H_\nu^{(1)\prime}(x) - J_\nu'(x)H_\nu^{(1)}(x) = \frac{2i}{\pi x}. \tag{C7}$$

For the $\vec{y}$ source point outside the circle, when $\vec{x}$ is inside the cavity, then

$$G(\vec{x},\vec{y}) = \sum_{m=-\infty}^{\infty} C_m J_m(nkr)e^{im(\theta-\phi)} \tag{C8}$$

and when $\vec{x}$ is outside the circle, then

$$G(\vec{x},\vec{y}) = \sum_{m=-\infty}^{\infty} D_m H_m^{(1)}(kr)e^{im(\theta-\phi)} + \frac{1}{4i}H_0^{(1)}(k|\vec{x}-\vec{y}|). \tag{C9}$$

Constants C_m and D_m are computed exactly as A_m and B_m:

$$C_m = -\frac{1}{2\pi x\Delta_m}H_m^{(1)}(k\rho),$$

$$D_m = -\frac{J_m(nx)}{2\pi x\Delta_m H_m^{(1)}(x)}H_m^{(1)}(k\rho) - \frac{J_m(x)}{4iH_m(x)}H_m^{(1)}(k\rho).$$

The final expressions of the Green function follow from the above formulas.

When the $\vec{y}$ source point is inside the circle, the plane is divided into three parts: (1) $r<\rho$, (2) $\rho<r<R$, and (3) $R<r$. Denoting the Green function in these regions by the corresponding numbers, it can be written as

$$G_j(\vec{x},\vec{y}) = \sum_{p=0}^{\infty} g_p^{(j)}(r,\rho)\cos[p(\theta-\phi)], \tag{C10}$$

where

$$g_p^{(1)}(r,\rho) = -\frac{1}{2\pi x}\epsilon_p \frac{J_p(nkr)J_p(nk\rho)}{J_p^2(nx)S_p(x)} + \frac{1}{4i}\epsilon_p \frac{J_p(knr)}{J_p(nx)} \times [H_p^{(1)}(kn\rho)J_p(nx) - H_p^{(1)}(nx)J_p(kn\rho)],$$

$$g_p^{(2)}(r,\rho) = -\frac{1}{2\pi x}\epsilon_p \frac{J_p(nkr)J_p(nk\rho)}{J_p^2(nx)S_p(x)} + \frac{1}{4i}\epsilon_p \frac{J_p(kn\rho)}{J_p(nx)} \times [H_p^{(1)}(knr)J_p(nx) - H_p^{(1)}(nx)J_p(knr)],$$

$$g_p^{(3)}(r,\rho) = -\frac{1}{2\pi x}\epsilon_p \frac{J_p(nk\rho)H_p^{(1)}(kr)}{J_p(nx)H_p^{(1)}(x)S_p(x)},$$

where ϵ_p was defined in Eq. (B6).

When point $\vec{y}$ is outside the circle, the plane is divided into three different regions: (1) $r<R$, (2) $R<r<\rho$, and (3) $\rho<r$. With the same notation as above, the Green function can be written

$$\tilde{G}_j(\vec{x},\vec{y}) = \sum_{p=0}^{\infty} \tilde{g}_p^{(j)}(r,\rho)\cos[p(\theta-\phi)], \tag{C11}$$

where

$$\tilde{g}_p^{(1)}(r,\rho) = -\frac{1}{2\pi x}\epsilon_p \frac{J_p(nkr)H_p^{(1)}(k\rho)}{J_p(nx)H_p^{(1)}(x)S_p(x)},$$

$$\tilde{g}_p^{(2)}(r,\rho) = -\frac{1}{2\pi x}\epsilon_p \frac{H_p^{(1)}(kr)H_p^{(1)}(k\rho)}{H_p^{(1)2}(x)S_p(x)} + \frac{1}{4i}\epsilon_p \frac{H_p^{(1)}(k\rho)}{H_p^{(1)}(x)} \times [H_p^{(1)}(x)J_p(kr) - H_p^{(1)}(kr)J_p(x)],$$

$$\tilde{g}_p^{(3)}(r,\rho) = -\frac{1}{2\pi x}\epsilon_p \frac{H_p^{(1)}(kr)H_p^{(1)}(k\rho)}{H_p^{(1)2}(x)S_p(x)} + \frac{1}{4i}\epsilon_p \frac{H_p^{(1)}(kr)}{H_p^{(1)}(x)} \times [H_p^{(1)}(x)J_p(k\rho) - H_p^{(1)}(k\rho)J_p(x)].$$

Notice that $G_1(\vec{x},\vec{y})=G_2(\vec{y},\vec{x})$, $G_3(\vec{x},\vec{y})=\tilde{G}_1(\vec{y},\vec{x})$, and $\tilde{G}_2(\vec{x},\vec{y})=\tilde{G}_3(\vec{y},\vec{x})$. It means that in all cases the Green function is symmetric: $G(\vec{x},\vec{y})=G(\vec{y},\vec{x})$ as it should be (see, e.g., [14]).

APPENDIX D: THREE DEGENERATE LEVELS

For three quasidegenerate levels, instead of Eq. (83) one gets the 3×3 determinant

$$\begin{vmatrix} \delta x - s_1 & A_{12} & A_{13} \\ A_{21} & \delta x - s_2 & A_{23} \\ A_{31} & A_{32} & \delta x - s_3 \end{vmatrix} = 0, \tag{D1}$$

which leads to the cubic equation

$$(\delta x)^3 - \sigma_1(\delta x)^2 + (\sigma_2 - \alpha)\delta x - \sigma_3 + \beta = 0. \tag{D2}$$

Here σ_i are the elementary symmetric functions of s_i,

$$\sigma_1 = s_1 + s_2 + s_3, \quad \sigma_2 = s_1 s_2 + s_2 s_3 + s_3 s_1, \quad \sigma_3 = s_1 s_2 s_3,$$

and (because $A_{ij}=A_{ji}$)

$$\alpha = A_{12}^2 + A_{23}^2 + A_{31}^2,$$

$$\beta = 2A_{12}A_{23}A_{31} + s_1 A_{23}^2 + s_2 A_{31}^2 + s_3 A_{12}^2.$$

To solve Eq. (D2), the next steps are standard. The substitution

$$\delta x = y + \frac{1}{3}\sigma_1 \tag{D3}$$

transforms Eq. (D2) to the reduced form

$$y^3 + py + q = 0, \tag{D4}$$

where

$$p = -\frac{1}{3}\sigma_1^2 + \sigma_2 - \alpha, q = -\frac{2}{27}\sigma_1^3 + \frac{1}{3}\sigma_1\sigma_2 - \sigma_3 + \delta, \tag{D5}$$

with $\delta=\beta-\frac{1}{3}\sigma_1\alpha$. Finally after the transformation

$$y = z - \frac{p}{3z}, \tag{D6}$$

one gets the equation $z^3 - p^3/27z^3 + q = 0$ which is a quadratic equation in variable

$$w = z^3. \tag{D7}$$

Its solution is

$$w = -\frac{q}{2} \pm \sqrt{\frac{q^2}{4} + \frac{p^3}{27}}. \tag{D8}$$

Equations (D3) and (D6)–(D8) give the well known solution of the cubic equation (D2). The question is how to choose a branch which tends to s_1 when $A_{ij}\to 0$. The discriminant of this equation is

$$D \equiv \frac{q^2}{4} + \frac{p^3}{27} = d + \varepsilon, \tag{D9}$$

where

$$d = \frac{1}{4}\left(-\frac{2}{27}\sigma_1^3 + \frac{1}{3}\sigma_1\sigma_2 - \sigma_3\right)^2 + \frac{1}{27}\left(\sigma_2 - \frac{1}{3}\sigma_1^2\right)^3$$

and

$$\varepsilon = \frac{1}{4}\delta^2 + \frac{1}{2}\delta\left(-\frac{2}{27}\sigma_1^3 + \frac{1}{3}\sigma_1\sigma_2 - \sigma_3\right) - \frac{1}{27}\alpha^3 + \frac{1}{9}\alpha^2\left(\sigma_2 - \frac{1}{3}\sigma_1^2\right) - \frac{1}{9}\alpha\left(\sigma_2 - \frac{1}{3}\sigma_1^2\right)^2.$$

Using the identity

$$d = -\frac{1}{108}[(s_1 - s_2)(s_2 - s_3)(s_3 - s_1)]^2,$$

the expression (D8) can be transformed into

$$w = w_0 - \frac{1}{2}\delta + \frac{i}{6\sqrt{3}}(s_1 - s_2)(s_2 - s_3)(s_3 - s_1)\left[\sqrt{1 - \frac{108\varepsilon}{[(s_1 - s_2)(s_2 - s_3)(s_3 - s_1)]^2}} - 1\right],$$

where

$$w_0 = \frac{1}{27}\sigma_1^3 - \frac{1}{6}\sigma_1\sigma_2 + \frac{1}{2}\sigma_3 + \frac{i}{6\sqrt{3}}(s_1 - s_2)(s_2 - s_3)(s_3 - s_1) = \frac{1}{27}(s_1 + s_2 e^{-2\pi i/3} + s_3 e^{2\pi i/3})^3.$$

Finally the root of the cubic equation (D2) which tends to s_1 when $A_{ij} \to 0$ is

$$z = \frac{1}{3}s\left[1 - \frac{27\delta}{2s^3} + \frac{3\sqrt{3}i}{2s^3}(s_1 - s_2)(s_2 - s_3)(s_3 - s_1)\left(\sqrt{1 - \frac{108\varepsilon}{[(s_1 - s_2)(s_2 - s_3)(s_3 - s_1)]^2}} - 1\right)\right]^{1/3},$$

where $s = s_1 + s_2 e^{-2\pi i/3} + s_3 e^{2\pi i/3}$.

[1] *Optical Microcavities*, edited by K. Vahala (World Scientific, Singapore, 2005).

[2] E. Krioukov, D. J. W. Klunder, A. Driessen, J. Greve, and C. Otto, Opt. Lett. **27**, 512 (2002).

[3] C. Gmachl, F. Capasso, E. E. Narimanov, J. U. Nöckel, A. D. Stone, J. Faist, D. L. Sivco, and A. Y. Cho, Science **280**, 1556 (1998).

[4] J. D. Jackson, *Classical Electrodynamics* (Wiley, New York, 1962).

[5] C. Vassallo, *Optical Waveguide Concepts* (Eslevier, Amsterdam, 1991).

[6] M. Lebental, N. Djellali, C. Arnaud, J.-S. Lauret, J. Zyss, R. Dubertrand, C. Schmit, and E. Bogomolny, Phys. Rev. A (to be published).

[7] A. Erdélyi, *Higher Transcendental Functions* (McGraw-Hill, New York, 1955), Vol. 3.

[8] J. Nöckel, Ph.D. dissertation, Yale University, 1997 (unpublished).

[9] M. Hentschel and H. Schomerus, Phys. Rev. E **65**, 045603(R) (2002).

[10] C. Yeh, Phys. Rev. **135**, A1193 (1964).

[11] L. Kaminetzky and J. Keller, SIAM J. Appl. Math. **22**, 109 (1972).

[12] I. Braun, G. Ihlein, F. Laeri, J. U. Nöckel, G. Schulz-Ekloff, F. Schüth, U. Vietze, O. Weis, and D. Wöhrle, Appl. Phys. B: Lasers Opt. **70**, 335 (2000).

[13] J. Wiersig, J. Opt. A, Pure Appl. Opt. **5**, 53 (2003); Phys. Rev. A **67**, 023807 (2003).

[14] P. M. Morse and H. Feshbach, *Methods of Theoretical Physics* (McGraw-Hill, New York, 1953), Vol. II.

[15] M. V. Berry and M. Tabor, Proc. R. Soc. London, Ser. A **356**, 375 (1977).

[16] S. Tomsovic and D. Ullmo, Phys. Rev. E **50**, 145 (1994).

[17] V. Doya, O. Legrand, F. Mortessagne, and C. Miniatura, Phys. Rev. E **65**, 056223 (2002).

[18] M. Lebental, J.-S. Lauret, R. Hierle, and J. Zyss, Appl. Phys. Lett. **88**, 031108 (2006).

[19] S.-Y. Lee, S. Rim, J.-W. Ryu, T.-Y. Kwon, M. Choi, and C.-M. Kim, Phys. Rev. Lett. **93**, 164102 (2004).